Journal of Materials Chemistry A

Accepted Manuscript

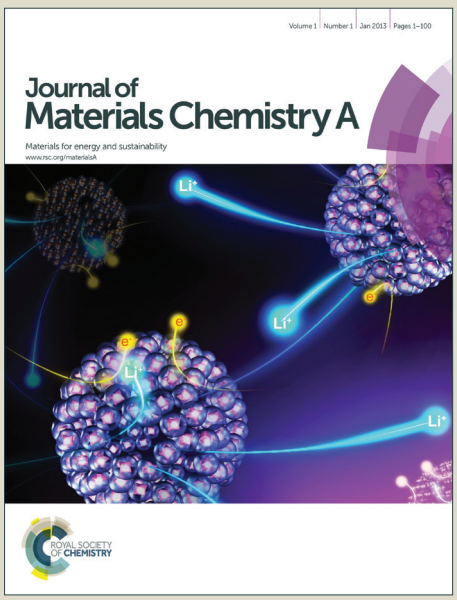

ROYAL SOCIETY OF CHEMISTRY

www.rsc.org/materialsA

Journal of Materials Chemistry A

Cite this: DOI: 10.1039/c0xx00000x

Paper

www.rsc.org/xxxxxx

High performance $LiMnPO_4$/C prepared by a crystallite size control method

Ming Zhao[a,b], Yu Fu[a], Ning Xu[b], Guoran Li[a], Mengtao Wu[b], and Xueping Gao[a]*

Received (in XXX, XXX) Xth XXXXXXXXX 20XX, Accepted Xth XXXXXXXXX 20XX
DOI: 10.1039/b000000x

A carbon matrix, which would restrict the growth of $LiMnPO_4$ crystallites, is built on the small Li_3PO_4 crystallites precipitated from aqueous solutions by the pyrolysis of sucrose. $LiMnPO_4$ is prepared with the carbon coated Li_3PO_4 as one of the reactant and the nuclei by a solvothermal method. It is demonstrated that the $LiMnPO_4$ with the smaller crystallite size (8-12 nm) on carbon matrix is successfully obtained by a crystallite size control method. As expected, the as-prepared $LiMnPO_4$/C sample presents desired electrochemical performance, including the higher discharge potential plateau, larger discharge capacity, excellent high rate capability, and good cycle stability. It is also confirmed that the smaller $LiMnPO_4$ crystallites on carbon matrix is beneficial to shorten the lithium ion diffusion path, and to increase the electrical conductivity of the $LiMnPO_4$/C sample, contributing to the improvement of the electrochemical superiority. The methodology described in this work is helpful to develop desired $LiMnPO_4$/C cathode materials for lithium ion batteries with high energy density.

Introduction

The rapid growing demands of lithium ion batteries with high energy and power density, low cost and high safety in stationary energy storage system, electric vehicles and power tools accelerate the research and development (R&D) of novel electro-active materials. It is noted that the performance of lithium ion batteries is largely determined by the cathode capacity and potential in the battery system. Among all cathode materials, olivine phosphates are considered to be more suitable in the application of power batteries based on their excellent thermal and electrochemical stability.[1-2] $LiFePO_4$ and $LiMnPO_4$ as cathode materials for lithium ion batteries were first reported by Goodenough's group in 1997,[3] which was regarded as a milestone in the development of cathode materials for lithium ion batteries. In comparison, $LiMnPO_4$ possesses the similar specific capacity, thermal and electrochemical stability to the commercial $LiFePO_4$. Differently, the operating potential plateau of $LiMnPO_4$ is about 4.1 V (vs. Li/Li^+), higher than that (3.6 V, vs. Li/Li^+) of $LiFePO_4$. It means that the output energy density of $LiMnPO_4$ cathode is higher as compared with $LiFePO_4$.

The main problem is that the intrinsic electronic conductivity and ionic conductivity are lower for $LiMnPO_4$, leading to slow R&D in the commercial progress of $LiMnPO_4$. In order to overcome the problem, more and more efforts are made in recent years. Commonly, the carbon coating is used to increase the electronic conductivity,[4-11] and cation substitution is introduced to increase the ionic conductivity.[12-18] Meanwhile, morphology and crystallite size control is also demonstrated to be effective for improving both the electronic and ionic conductivity of $LiMnPO_4$.[8-26] Especially, $LiMnPO_4$ with particular morphology, including spheres,[27,28] plates,[18,28-32] rods,[9,33,34] nanowires,[35,36] wedges,[37] flexible 3D-macroporous balls/flakes,[38] and flower-like microstructures,[39] presents very interesting structural and electrochemical characteristics. To shorten the ion diffusion path in the bulk, it is more favourite to use $LiMnPO_4$ with small crystallite size, which is usually prepared by different methods such as phosphate–formate precursor method,[40] ultrasonic spray pyrolysis method,[7] antisolvent precipitation method,[41] and hydrothermal method.[42] It is noted that both the small crystallite size and carbon coating are indispensable for $LiMnPO_4$ to achieve good electrochemical performance based on the improvement of the electronic conductivity and ion diffusion. Therefore, how to adjust crystallite size and carbon coating layer for $LiMnPO_4$/C is highly important.

In this work, from the practical consideration, a new approach is made to prepare $LiMnPO_4$ with small crystallite size by a facile and low cost precipitation, modified further by carbon coating using a solvothermal method.

Experimental

Preparation and characterizations

The Sample A was synthesized by a solvothermal procedure, in which Li_3PO_4 on a carbon frame reacted with Mn^{2+} in a mixture medium of deionized water and PEG400. The Li_3PO_4 was precipitated by slowly mixing the same volume LiOH (1.5 $mol•dm^{-3}$) and H_3PO_4 (0.5 $mol•dm^{-3}$) aqueous solution with peristaltic pumps. The precipitation was filtered, washed with deionized water, and dried under vacuum at 60 °C in sequence. The Li_3PO_4 was coated with carbon from sucrose (10 wt. %) by

ball milling, and then calcined at 550 °C for 2 h in an argon atmosphere. The resulting carbon-coated Li_3PO_4 was mixed with stoichiometric $MnSO_4$ in a solution with deionized water and PEG400 (1:1, volume ratio). Then, the mixture was heated in a Teflon-lined autoclave at 180 °C for 10 h. The solid was separated in centrifuge, washed with deionized water and alcohol, and dried under vacuum at 60 °C overnight. Finally, the solid was further coated with carbon by the same method as foregoing Li_3PO_4 with sucrose (25 wt. %). Sample B and C were prepared for comparison. The Sample B was synthesized by the same route to the Sample A, except the Li_3PO_4 was only heated without carbon coating under the same condition. Sample C was obtained by solvothermally treating the mixture of stoichiometric LiOH, H_3PO_4 and $MnSO_4$ (molar ratio 3:1:1) in the same medium and under the same condition as the Sample A. Then, the product was coated by carbon with the same parameters as the Sample A. All the reagents were of the analytical grade and used as received without any purification or other treatments. The structure and morphology of the Li_3PO_4 intermediates and the final products were characterized by powder X-ray diffraction (XRD, Rigaku Mini Flex II), scanning electron microscopy (SEM, Hitachi S4800), and transmission electron microscopy (TEM, FEI Tecnai G2 F20). The carbon content of the $LiMnPO_4$/C samples was measured on a high frequency infrared carbon and sulfur analyzer model CS-901B.

Electrochemical measurements

R2032 coin-type cells were assembled in an argon filled dry glove box to investigate the electrochemical performance of the materials. Lithium foil was used as counter and reference electrode, the solution of $LiPF_6$ (1 mol•dm^{-3}) in the mixture of propyl carbonate (PC), ethyl carbonate (EC) and dimethyl carbonate (DMC) (volume ration 1:1:1) was used as the electrolyte, and the Celgard 2300 was used as the separator. The working electrode was prepared as follow: the as-prepared $LiMnPO_4$ materials as the active materials, polyvinylidene fluoride (PVdF) as the binder, and Timcal Super P carbon black as the conductivity enhancer were mixed in the gravimetric ratio of 7:1:2 in N-methyl-2-pyrrolidone (NMP) to form a thick slurry. The slurry was then coated onto aluminum foil and dried under vacuum at 90 °C. Finally, the electrode sheet was pressed and cut to round pieces. Charge/discharge tests were performed on Lanhe CT2001A battery test systems and the cyclic voltammetry (CV) measurements were carried out on a Solartron SI 1287 electrochemical interface. All the tests were conducted at room temperature.

Results and discussion

Fig. 1 illustrates the schematic formation routes of the $LiMnPO_4$ crystallites on the carbon matrix. The different synthetical routes lead to the significant difference in the crystallite size of the $LiMnPO_4$ samples. In the scheme, the green, red and blue lines show the preparation routes of Sample A, B, and C, respectively. For Sample A and B, which are synthesized via a Li_3PO_4 precursor, Li_3PO_4 is produced by adding LiOH and H_3PO_4 aqueous solutions with a stoichiometric molar ratio of 3:1 to a reactor under vigorous stirring. Then, the precipitated Li_3PO_4 reacts with $MnSO_4$, followed by a carbon coating procedure to obtain Sample B. In the synthetical route of Sample A, the crystallites of the Li_3PO_4 precursor are coated with carbon by the pyrolysis of sucrose before reacting with Mn^{2+}. In particular, the carbon is coated on the surface of a single Li_3PO_4 crystallite and/or aggregates of several crystallites to fabricate a matrix, which would stabilize the crystallite size and prevent the formation of larger $LiMnPO_4$ crystallites or aggregates in the subsequent solvothermal procedure. During the subsequent solvothermal reaction, most Li_3PO_4 crystallites restricted by the carbon matrix react with Mn^{2+} to form small primary $LiMnPO_4$ crystallites, while some Li_3PO_4 aggregates in the carbon frame cell would produce larger $LiMnPO_4$ crystallites with the manganese ions. Also, the resulted $LiMnPO_4$ is finally coated by carbon to obtain Sample A. Under the solvothermal condition, the carbon frame would be weakened, leading to the formation of larger sized $LiMnPO_4$ crystallites as compared with the Li_3PO_4 precursor. As a result of restriction of the carbon matrix on the Li_3PO_4 precursor, the crystallite size of Sample A is smaller than that of Sample B. As shown in the figure, Sample C is prepared by directly mixing the raw material in a stoichiometric ratio and then solvothermal treatment followed by the same carbon coating procedure as Sample A and B. Without any restriction, the crystallite size of Sample C is larger than the other two samples.

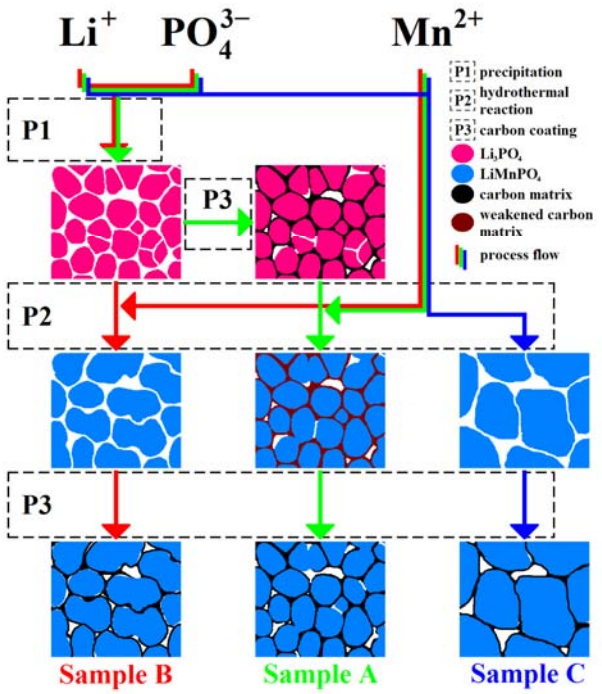

Fig. 1 Schematic diagram of the preparation routes of the $LiMnPO_4$/C samples.

The powder X-ray diffraction measurements are carried out to characterize the structure and crystallite size of the Li_3PO_4 intermediates and $LiMnPO_4$ samples. The XRD patterns and their fitting results are shown in Fig. 2. Fig. 2a presents XRD patterns of the as-precipitated, heat treated and carbon coated Li_3PO_4, respectively. The diffraction peaks in the three samples are assigned to the orthorhombic structure of Li_3PO_4 (space group *P*mn21(31)), matched perfectly with JCPDS PDF card 25-1030. No peaks of the impurities are detected. In addition, there are no

corresponding signals of carbon due to the amorphous state existed in the sample. The profiles of the three sets of experimental data are quite similar. The calculated lattice constants and crystallite size of the samples are listed in Table 1. Obviously, there are no significant changes in the lattice constants and crystalline size (about 14 nm), indicating that the structure and crystalline state of Li_3PO_4 are stable in the carbon coating procedure.

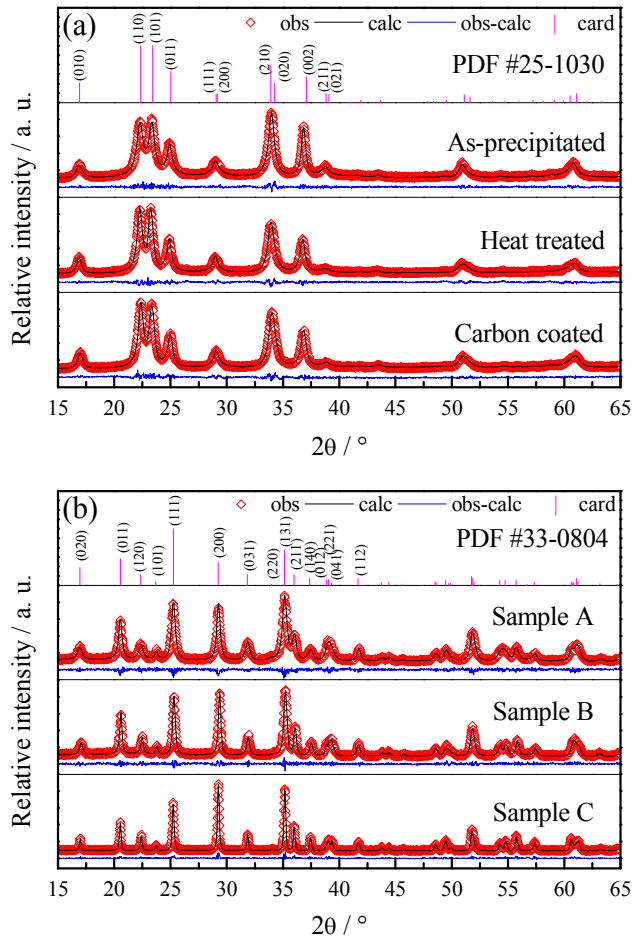

Fig. 2 XRD patterns of Li_3PO_4 intermediates (a) and $LiMnPO_4$/C samples (b).

XRD patterns of the $LiMnPO_4$/C samples are shown in Fig. 2b. The diffraction peaks of all the samples are assigned to the orthorhombic structure (space group *P*mnb(62), JCPDS PDF 33-0804). Meanwhile, the diffraction peaks of the impurities and coating carbon are still not detected. The carbon contents are 5.37, 5.55, and 5.21wt % for Sample A, B, and C, respectively. Nevertheless, the noticeable difference is that the width of the diffraction peaks of the $LiMnPO_4$ samples is reduced obviously from Sample A to Sample C. The calculated lattice constants and crystallite size of $LiMnPO_4$ samples are also summarized in Table 1. Apparently, the lattice constants are almost identical, suggesting the same crystallographic structure of the three $LiMnPO_4$ samples. Differently, the average crystallite sizes are varied remarkably for the $LiMnPO_4$ samples, which are increased from 15.4 nm (Sample A) to 31.3 nm (Sample B) and 50.7 nm (Sample C), respectively. It means that the crystallite size of $LiMnPO_4$ can be adjusted by the different preparation route, further leading to the variation of the electrochemical performance of $LiMnPO_4$/C samples.

Table 1 Lattice constants and crystallite size of the as-prepared Li_3PO_4 precursors and $LiMnPO_4$ samples. The crystallite size is calculated by the Scherrer equation.

Parameter / unit	*a* / nm	*b* / nm	*c* / nm	Crystallite size / nm
JCPDS (Li_3PO_4) PDF 25-1030	0.61155	0.5234	0.48452	n/a
As-precipitated Li_3PO_4	0.61197	0.52475	0.48611	14.4
Heat treated Li_3PO_4	0.61366	0.52470	0.48806	14.3
Carbon coated Li_3PO_4	0.61226	0.52181	0.48596	13.8
JCPDS ($LiMnPO_4$) PDF 33-0804	0.6106	1.0454	0.4749	n/a
$LiMnPO_4$ Sample A	0.60976	1.04490	0.47476	15.4
$LiMnPO_4$ Sample B	0.60851	1.03808	0.47325	31.3
$LiMnPO_4$ Sample C	0.61024	1.04211	0.47425	50.7

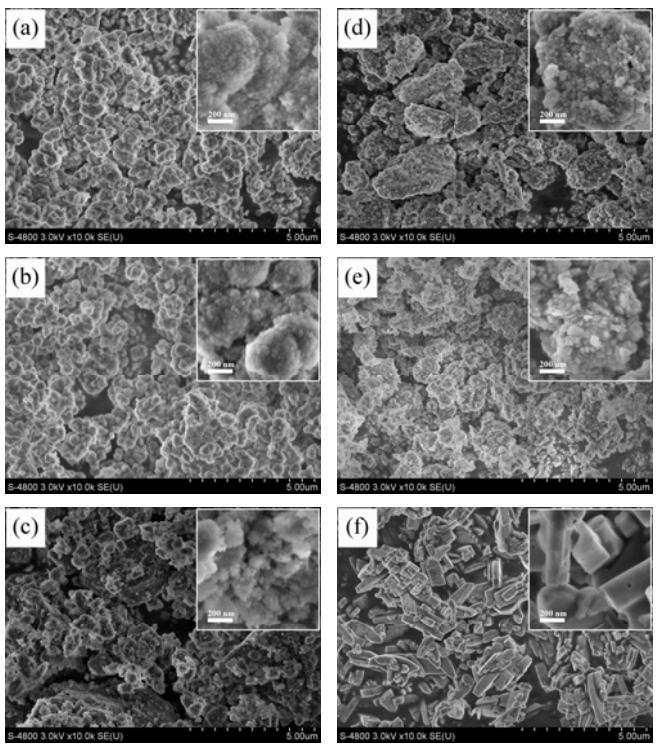

Fig. 3 SEM images of the as-precipitated Li_3PO_4 (a), heat treated Li_3PO_4 (b), carbon coated Li_3PO_4 (c), Sample A (d), Sample B (e), and Sample C (f).

SEM images of the Li_3PO_4 intermediates and $LiMnPO_4$/C samples are shown in Fig. 3. The insets show the details at a higher magnification. The large secondary particles of Li_3PO_4

consist of nanosized primary crystallites. Specifically, the as-precipitated Li_3PO_4 exist as sphere-like morphology (Fig. 3a). For the heat treated Li_3PO_4, a few of secondary particles is divided into smaller pieces, which are reconstructed to form new secondary particles with irregular morphology (Fig. 3b). In the case of the carbon coated Li_3PO_4 (Fig. 3c), the spherical morphology of the as-precipitated Li_3PO_4 secondary particles is partially destroyed and new secondary particles are formed during the carbon coating procedure. The results suggest that the large secondary particles of Li_3PO_4 precursors are not very compact, and would be varied in morphology under thermal and/or mechanical treatments. In agreement with the XRD analysis, the primary grains of Li_3PO_4 are almost identical in all the cases.

When $LiMnPO_4$ samples are prepared, the morphology of secondary particles and crystallite size of $LiMnPO_4$ are dramatically different (Fig. 3d, e and f). Firstly, Sample A exists as looser aggregates, consisted with smaller primary crystallites as compared with Sample B. In particular, the rough surfaces and porous structure can be observed for Sample A and Sample B, which are beneficial to the wettability of the active materials with electrolyte, and the diffusion of electrolyte inside secondary particles. Furthermore, the charge-transfer process can be facilitated on the rough surface of smaller primary crystallites. In contrast, large slab-like particles with a smooth surface are shown for Sample C, which are not helpful in the electrochemical performance of $LiMnPO_4$. It is noted that the primary crystallite size is 50.7 nm from XRD analysis by the Scherrer equation, which is smaller than the particle size (200~500 nm) from SEM image (Fig. 3f). It means that secondary slab-like particles are consisted of tightly connected primary crystallites for Sample C. Here, the large crystallite size and particle size of Sample C are mainly attributed to the limitless growth of $LiMnPO_4$. While, the small crystallite size of the Sample A and Sample B is formed due to the restriction on the growth of $LiMnPO_4$, arised from the small Li_3PO_4 crystallites.

The more clear observation of the $LiMnPO_4$ crystallites on carbon matrix for Sample A is shown in TEM images (Fig. 4). Firstly, the small and homogeneous Li_3PO_4 crystallites with a size of 8-12 nm can be found, almost in agreement with XRD analysis. In particular, the carbon films by the pyrolysis of sucrose are coated on the surface of Li_3PO_4 crystallites. The manganese ion could pass through amorphous carbon films to form $LiMnPO_4$ crystallites. Generally, the primary crystallite size of $LiMnPO_4$ (about 15 nm for Sample A) is larger than the Li_3PO_4 precursor, because of the flexibility of the coated carbon matrix, intrinsic volume expansion of the reaction and the agglomeration by several Li_3PO_4 crystallites in one vessel of the matrix. It means that the further growth of the Sample A is restricted by the carbon coating film, acting as a seperator to prevent the Li_3PO_4 crystallites from contacting and/or forming large $LiMnPO_4$ crystallites. Therefore, the smallest crystallite size of Sample A is obtained due to the small Li_3PO_4 nuclei and the coated carbon frames, which would shorten the distance of lithium ion diffusion and increase the apparent electronic conductivity.

The electrochemical performance of the $LiMnPO_4$/C samples is evaluated by galvanostatic charge/discharge tests at room temperature. The test sequence is: constant current charge, constant potential charge, rest, constant current discharge, rest and loop. The C-rate standard is 1 C = 171 $mA•g^{-1}$ based on the theoretical specific capacity of $LiMnPO_4$ (171 $mAh•g^{-1}$). The constant charge current rate is 0.1 C and the constant discharge current rates are 0.05 C to 5 C. The potential range is set to be from 4.5 to 2.5 V (vs Li/Li^+). The constant potential charge time and rest time are 3.5 h and 5 min, respectively. As illustrated in Fig. 5, the maximum discharge capacity of Sample A is 153.9 $mAh•g^{-1}$ at 0.05C rate, larger than that of Sample B (127.8 $mAh•g^{-1}$) and C (61 $mAh•g^{-1}$), respectively. Moreover, the good cycle stability is also obtained for Sample A at various rates.

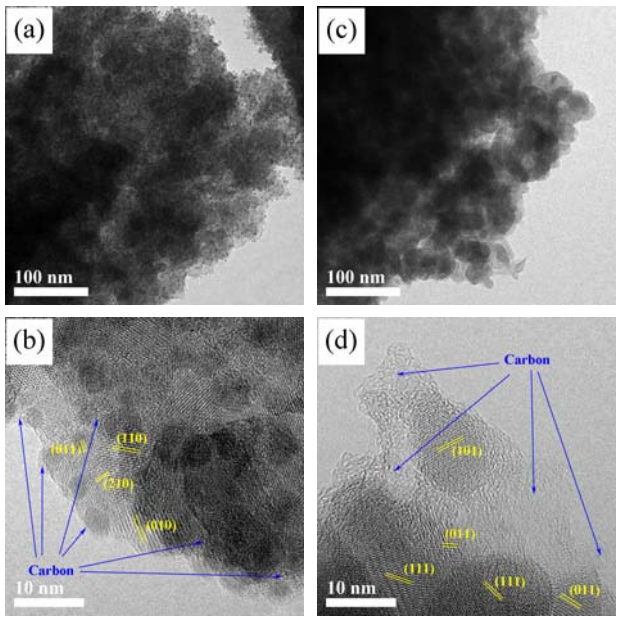

Fig. 4 TEM images of the carbon coated Li_3PO_4 (a, b) and the $LiMnPO_4$/C Sample A (c, d) at different magnifications.

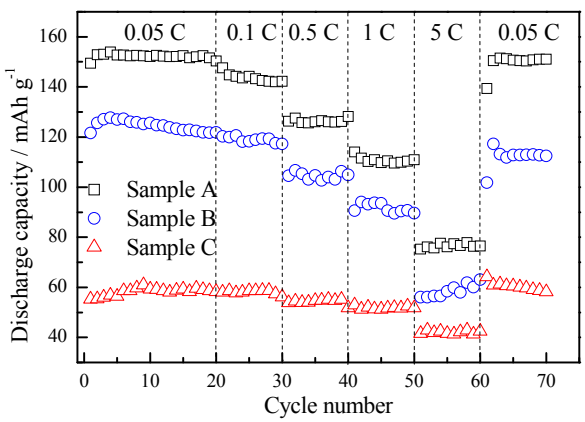

Fig. 5 The discharge capacity of the $LiMnPO_4$/C samples at different discharge rates.

The charge/discharge cycle profiles of the three $LiMnPO_4$/C samples are compared in Fig. 6. The cycle numbers are corresponding to the same cycles in Fig. 5. Clearly, Sample A presents the relatively high and flat discharge potential plateau of 4.1V (vs Li/Li^+), larger initial discharge capacity of above 150 $mAh•g^{-1}$, and larger coulombic efficiency of 72.4 %. In the following cycles at various discharge rates, Sample A still shows advantages on discharge capacity, high-rate capability, and electrochemical polarization in the charge/discharge process.

Except the initial cycle, the coulombic efficiency of all the $LiMnPO_4$ samples is near 100 %. Commonly, the discharge potential is inevitably dropped while the discharge rate is increased, because of the ohmic IR potential drop and the electrochemical polarization. At high discharge rates, the discharge potential plateau is sloped. When the discharge rate of is restored to 0.05 C rate in the 65th cycle, The relatively high and flat potential plateau is still observed for Sample A with no noticeable capacity loss, while Sample B shows more obvious capacity decay. For Sample C, the electrochemical performance is slightly improved after 65 cycles due to the activation during cycling.

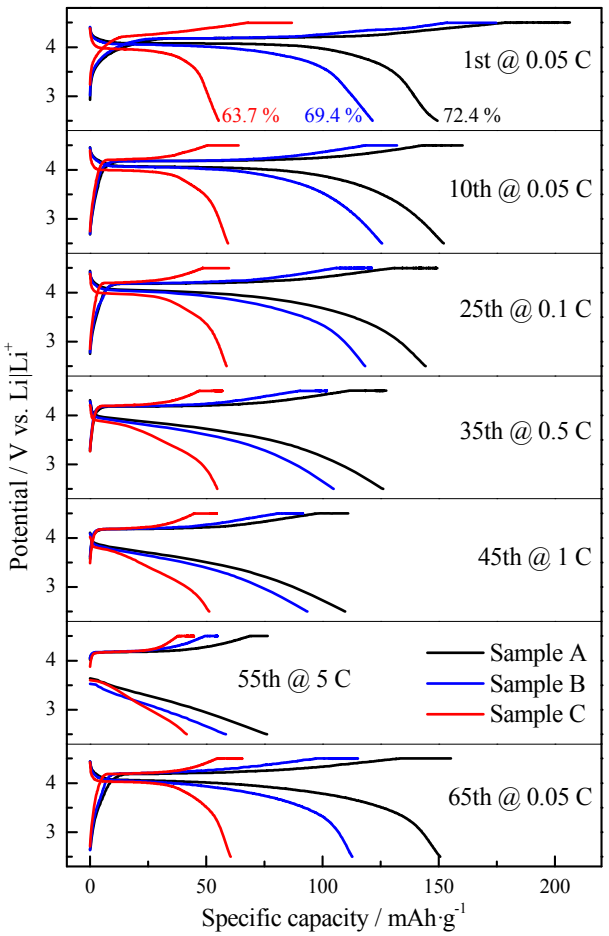

Fig. 6 The charge/discharge curves of the $LiMnP_4$/C samples at different cycles corresponding to Fig. 5.

The CV measurements are conducted to further investigate the reversibility of the electrochemical reaction of the $LiMnPO_4$/C samples during cycling. Fig. 7 presents the CV profiles of the $LiMnPO_4$/C samples, and the peak potential/current information is collected in Table 2. The symmetric lithium ion deintercalation (anodic) and intercalation (cathodic) peaks are obtained for Sample A and Sample B at different scan rates. With increasing the scan rate, the anodic peaks move to the high potential direction, the cathodic peaks shift to the low potential direction, accompanied with the increase of the peak current density. For Sample C, the anodic peaks are not detected at high scan rates of 0.2 and 0.5 mV•s^{-1} due to the large electrochemical polarization. In comparison, Sample A delivers the lower electrochemical polarization and high electrochemical activity, resulting in the larger discharge capacity, excellent high rate capability, and good cycle stability as mentioned above.

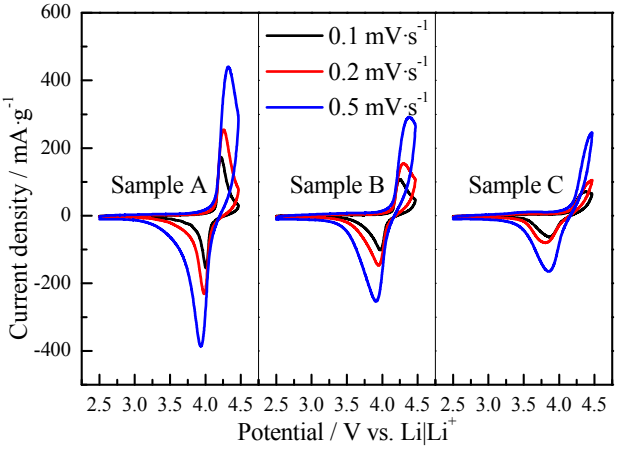

Fig. 7 CV profiles of the $LiMnPO_4$/C samples at different scan rates.

Table 2 The information from the CV peaks of the $LiMnPO_4$/C samples*.

		Sample A		Sample B		Sample C	
		E	***j***	***E***	***j***	***E***	***j***
0.1 mV·s^{-1}	A	4.219	173.1	4.247	107.2	4.371	70.9
	C	4.006	-155.2	3.972	-101.8	3.866	-63.4
0.2 mV·s^{-1}	A	4.255	254.2	4.299	154.3	n/a	n/a
	C	3.982	-231.5	3.946	-146.7	3.804	-80.1
0.5 mV·s^{-1}	A	4.317	439.9	4.383	291.7	n/a	n/a
	C	3.936	-386.4	3.911	-253.7	3.855	-164.7

*$\boldsymbol{E}$ = Peak potential in V vs. Li/Li^+, $\boldsymbol{j}$ = Peak current density in mA·g^{-1}, A = Anodic peak and C = Cathodic peak.

Randles-Sevcik equation (Eq. (1)), which describes the dependence of the peak current density with the characteristics of the electrode, is applied to intuitively compare the CV results.

$$j_p = kF^{3/2}R^{-1/2}T^{-1/2}ACD^{1/2}v^{1/2} \quad \text{Eq. (1)}$$

Where j_p is the gravimetric peak current density, k is a constant, F is the Faraday constant, R is the ideal gas constant, T is the temperature, A is the area of the electrode contacting with the electrolyte, C is the concentration of the lithium ion in the testing electrode, D is the diffusion coefficient of the lithium ion in the active substance $LiMnPO_4$, and v is the scan rate, respectively. Under a certain testing condition, k, F, R, T and C are constant. Let $K = kF^{3/2}R^{-1/2}T^{-1/2}C$, Eq. (1) can be reduced to Eq. (2).

$$j_p = KAD^{1/2}v^{1/2} \quad \text{Eq. (2)}$$

Fig. 8 shows the peak current density of the $LiMnPO_4$ samples versus the square root of the scan rate. The linear fittings with fixed intercepts of zero's are performed. The fitting results are summarized in Table 3. The results show good linearity with R^2 value near 1. For Sample A and B, the slope of the anodic peaks is similar to the cathodic peaks, respectively, illustrating the good reversibility. Differently, the absolute value of the slope of

Sample A is larger than that of Sample B and C (cathodic only for Sample C). From Eq. (2), it is known that the slope is determined by two variables of *A* and *D*. Here, *D* is a constant inside $LiMnPO_4$ crystallites. It means that the reactive surface area of Sample A is reasonably larger, in consistent with the XRD analysis and TEM observation. Therefore, the large slope implies the better electrochemical performance. The linear fitting results are comparable with Cao et al's work[43]. The data obtained from CVs suggest the highest reversibility of Sample A.

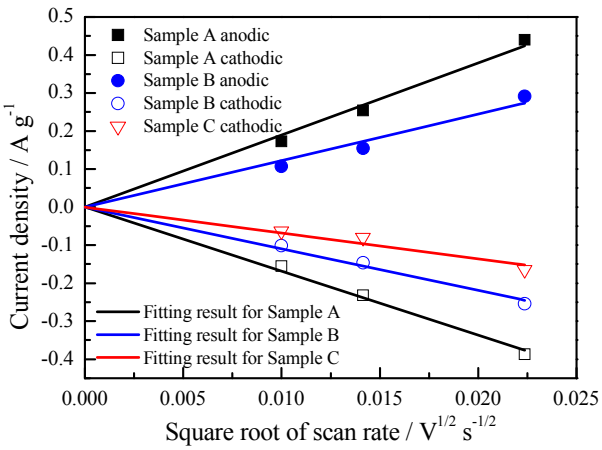

Fig. 8 The relationship between peak current density and the square root of the scan rate.

Table 3 The linear fitting results of the dependence of the current density versus the square root of the scan rate.

		Slope	R^2
Sample A	Anodic	18.95	0.997
	Cathodic	-16.83	0.998
Sample B	Anodic	12.22	0.990
	Cathodic	-10.96	0.997
Sample C	Cathodic	-6.812	0.984

Conclusions

$LiMnPO_4$ with small crystallite size is successfully synthesized by a precipitation-solvothermal method. Here, the Li_3PO_4 precursors are coated with carbon, further restricting the subsequent growth of the $LiMnPO_4$ crystallites on the carbon matrix. Correspondingly, the $LiMnPO_4$/C sample with the smaller $LiMnPO_4$ crystallite size presents the higher potential plateau, larger discharge capacity, excellent high rate capability, and good cycle stability. The strategy described in this work is helpful for the practical applications of $LiMnPO_4$ cathode in LIBs.

Acknowledgements

This work is supported by NSFC (51272108), Research Fund for the Doctoral Program of Higher Education (20120031130002) and MOE Innovation Team (IRT13022) of China. The authors also wish to express their sincere thanks to Mr. Song and Ms. Fu from Bamo Tech for helpful discussion.

Notes and references

[a] *Institute of New Energy Material Chemistry, Collaborative Innovation Center of Chemical Science and Engineering (Tianjin), Tianjin Key Laboratory of Metal and Molecule Based Material Chemistry, Nankai University, Tianjin 300071, China. Fax: +86-22-23500876; Tel: +86-22-23500876; E-mail: xpgao@nankai.edu.cn*
[b] *Tianjin Bamo Tech Co., Ltd., Tianjin 300384, China.*

1 V. Aravindan, J. Gnanaraj, Y. S. Lee and S. Madhavi, $LiMnPO_4$ – A next generation cathode material for lithium-ion batteries, *J. Mater. Chem. A*, 2013, **1**, 3518.
2 D. Choi, J. Xiao, Y. J. Choi, J. S. Hardy, M. Vijayakumar, M. S. Bhuvaneswari, J. Liu, W. Xu, W. Wang, Z. G. Yang, G. L. Graff and J. G. Zhang, Thermal stability and phase transformation of electrochemically charged/discharged $LiMnPO_4$ cathode for Li-ion batteries, *Energy Environ. Sci.*, 2011, **4**, 4560.
3 A. K. Padhi, K. S. Nanjundaswamyand and J. B. Goodenough, Phospho-olivines as positive-electrode materials for rechargeable lithium batteries, *J. Electrochem. Soc.*, 1997, **144**, 1188.
4 J. S. Yang and J. J. Xu, Synthesis and characterization of carbon-coated lithium transition metal phosphates $LiMPO_4$ (M = Fe, Mn, Co, Ni) prepared via a nonaqueous sol-gel route, *J. Electrochem. Soc.*, 2006, **153**, A716.
5 Z. Bakenov and I. Taniguchi, Physical and electrochemical properties of $LiMnPO_4$/C composite cathode prepared with different conductive carbons, *J. Power Sources*, 2010, **195**, 7445.
6 T. N. L. Doan, Z. Bakenov and I. Taniguchi, Preparation of carbon coated $LiMnPO_4$ powders by a combination of spray pyrolysis with dry ball-milling followed by heat treatment, *Adv. Powder Tech.*, 2010, **21**, 187.
7 S. M. Oh, S. W. Oh, C. S. Yoon, B. Scrosati, K. Amine and Y. K. Sun, High-performance carbon-$LiMnPO_4$ nanocomposite cathode for lithium batteries, *Adv. Funct. Mater.*, 2010, **20**, 3260.
8 H. Guo, C. Y. Wu, J. Xie, S. C. Zhang, G. S. Cao and X. B. Zhao, Controllable synthesis of high-performance $LiMnPO_4$ nanocrystals by a facile one-spot solvothermal process, *J. Mater. Chem. A*, 2014, **2**, 10581.
9 P. R. Kumar, M. Venkateswarlu, M. Misra, A. K. Mohanty and N. Satyanarayana, Carbon coated $LiMnPO_4$ nanorods for lithium batteries, *J. Electrochem. Soc.*, 2011, **158**, A227.
10 S. Moon, P. Muralidharan and D. K. Kim, Carbon coating by high-energy milling and electrochemical properties of $LiMnPO_4$ obtained in polyol process, *Ceram. Int.*, 2012, **38S**, S471.
11 J. L. Liu, X. Y. Liu, T. Huang and A. S. Yu, Synthesis of nano-sized $LiMnPO_4$ and in situ carbon coating using a solvothermal method, *J. Power Sources*, 2013, **229**, 203.
12 J. W. Lee, M. S. Park, B. Anass, J. H. Park, M. S. Paik and S. G. Doo, Electrochemical lithiation and delithiation of $LiMnPO_4$: Effect of cation substitution, *Electrochimica Acta*, 2010, **55**, 4162.
13 D. Y. Wang, C. Y. Ouyang, T. Drézen, I. Exnar, A. Kay, N. H. Kwon, P. Gouerec, J. H. Miners, M. K. Wang and M. Gratzel, Improving the electrochemical activity of $LiMnPO_4$ via Mn-site substitution, *J. Electrochem. Soc.*, 2010, **157**, A225.
14 G. Y. Chen, A. K. Shukla, X. Y. Song and T. J. Richardson, Improved kinetics and stabilities in Mg-substituted $LiMnPO_4$, *J. Mater. Chem.*, 2011, **21**, 10126.
15 J. F. Ni and L. J. Gao, Effect of copper doping on $LiMnPO_4$ prepared via hydrothermal route, *J. Power Sources*, 2011, **196**, 6498.
16 G. Yang, H. Ni, H. D. Liu, P. Gao, H. M. Ji, S. Roy, J. Pinto and X. F. Jiang, The doping effect on the crystal structure and electrochemical properties of $LiMn_xM_{1-x}PO_4$ (M = Mg, V, Fe, Co, Gd), *J. Power Sources*, 2011, **196**, 4747.
17 Z. Yang, G. S. Cao, J. Xie, and X. B. Zhao, Oleic acid-assisted preparation of $LiMnPO_4$ and its improved electrochemical performance by Co doping, *J. Solid State Electrochem.*, 2012, **16**, 1271.
18 Y. Z. Dong, H. Xie, J. Song, M. W. Xu, Y. M. Zhao and J. B. Goodenough, The prepared and electrochemical property of Mg doped $LiMnPO_4$ nanoplates as cathode materials for lithium-ion batteries *J. Electrochem. Soc.*, 2012, **159**, A995.
19 N. H. Kwon, T. Drezen, I. Exnar, I. Teerlinck, M. Isono and M. Graetzel, Enhanced electrochemical performance of mesoparticulate $LiMnPO_4$ for lithium ion batteries, *Electrochem. Solid-State Lett.*, 2006, **9**, A277.

20 T. Drezen, N. H. Kwon, P. Bowen, I. Teerlinck, M. Isono and I. Exnar, Effect of particle size on $LiMnPO_4$ cathodes, *J. Power Sources*, 2007, **174**, 949.

21 C. Liu, X. H. Wu, W. W. Wu, J. C. Cai and S. Liao, Preparation of nanocrystalline $LiMnPO_4$ via a simple and novel method and its isothermal kinetics of crystallization, *J. Mater. Sci.*, 2011, **46**, 2474.

22 P. Barpanda, K. Djellab, N. Recham, M. Armand and J. M. Tarascon, Direct and modified ionothermal synthesis of $LiMnPO_4$ with tunable morphology for rechargeable Li-ion batteries, *J. Mater. Chem.*, 2011, **21**, 10143.

23 K. Dokko, T. Hachida and M. Watanabe, $LiMnPO_4$ nanoparticles prepared through the reaction between Li_3PO_4 and molten aqua-complex of $MnSO_4$, *J. Electrochem. Soc.*, 2011, **158**, A1275.

24 H. M. Ji, G. Yang, H. Ni, S. Roy, J. Pinto and X. F. Jiang, General synthesis and morphology control of $LiMnPO_4$ nanocrystals via microwave-hydrothermal route, *Electrochimica Acta*, 2011, **56**, 3093.

25 D. Rangappa, K. Sone, Y. Zhou, T. Kudo and I. Honma, Size and shape controlled $LiMnPO_4$ nanocrystals by a supercritical ethanol process and their electrochemical properties, *J. Mater. Chem.*, 2011, **21**, 15813.

26 T. H. Kim, H. S. Park, M. H. Lee, S. Y. Lee and H. K. Song, Restricted growth of $LiMnPO_4$ nanoparticles evolved from a precursor seed, *J. Power Sources*, 2012, **210**, 1.

27 Z. Bakenov and I. Taniguchi, Synthesis of spherical $LiMnPO_4$/C composite microparticles, *Mater. Res. Bull.*, 2011, **46**, 1311.

28 W. Liu, P. G. Gao, Y. Y. Mi, J. T. Chen, H. H. Zhou and X. X. Zhang, Fabrication of high tap density $LiFe_{0.6}Mn_{0.4}PO_4$/C microspheres by a double carbon coating–spray drying method for high rate lithium ion batteries, *J. Mater. Chem. A*, 2013, **1**, 2411.

29 D. W. Choi, D. H. Wang, I. T. Bae, J. Xiao, Z. M. Nie, W. Wang, V. V. Viswanathan, Y. J. Lee, J. G. Zhang, G. L. Graff, Z. G. Yang and J. Liu, $LiMnPO_4$ nanoplate grown via solid-state reaction in molten hydrocarbon for Li-ion battery cathode, *Nano Lett.*, 2010, **10**, 2799.

30 V. Koleva, E. Zhecheva and R. Stoyanova, Facile synthesis of $LiMnPO_4$ olivines with a plate-like morphology from a dittmarite-type $KMnPO_4 \cdot H_2O$ precursor, *Dalton Trans.*, 2011, **40**, 7385.

31 Y. Z. Dong, L. Wang, S. L. Zhang, Y. M. Zhao, J. P. Zhou, H. Xie and J. B. Goodenough, Two-phase interface in $LiMnPO_4$ nanoplates, *J. Power Sources*, 2012, **215**, 116.

32 X. L. Pan, C. Y. Xu, D. Hong, H. T. Fang and L. Zhen, Hydrothermal synthesis of well-dispersed $LiMnPO_4$ plates for lithium ion batteries cathode, *Electrochimica Acta*, 2013, **87**, 303.

33 H. L. Wang, Y. Yang, Y. Y. Liang, L. F. Cui, H. S. Casalongue, Y. G. Li, G. S. Hong, Y. Cui and H. J. Dai, $LiMn_{1-x}Fe_xPO_4$ nanorods grown on graphene sheets for ultrahigh-rate-performance lithium ion batteries, *Angew. Chem. Int. Ed.*, 2011, **50**, 7364.

34 P. R. Kumar, M. Venkateswarlu, M. Misra, A. K. Mohanty and N. Satyanarayana, Enhanced conductivity and electrical relaxation studies of carbon-coated $LiMnPO_4$ nanorods, *Ionics*, 2013, **19**, 461.

35 Q. Lu, G. S. Hutchings, Y. Zhou, H. L. Xin, H. M. Zheng and F. Jiao, Nanostructured flexible Mg-modified $LiMnPO_4$ matrix as high-rate cathode materials for Li-ion batteries, *J. Mater. Chem. A*, 2014, **2**, 6368.

36 Z. Z. Pei, X. Zhang and X. Gao, Shape-controlled synthesis of $LiMnPO_4$ porous nanowires, *J. Alloys and Compd.*, 2013, **546**, 92.

37 Z. Gao, X. L. Pan, H. P. Li, S. K. Xie, R. X. Yi and W. Jin, Hydrothermal synthesis and electrochemical properties of dispersed $LiMnPO_4$ wedges, *Cryst. Eng. Comm.*, 2013, **15**, 7808.

38 H. C. Yoo, M. K. Jo, B. S. Jin, H. S. Kim and J. Cho, Flexible morphology design of 3D-macroporous $LiMnPO_4$ cathode materials for Li secondary batteries: ball to flake, *Adv. Energy Mater.*, 2011, **1**, 347.

39 P. Nie, L. F. Shen, F. Zhang, L. Chen, H. F. Deng and X. G. Zhang, Flower-like $LiMnPO_4$ hierarchical microstructures assembled from single-crystalline nanosheets for lithium-ion batteries, *Cryst. Eng. Comm.*, 2012, **14**, 4284.

40 V. Koleva, R. Stoyanova and E. Zhecheva, Nano-crystalline $LiMnPO_4$ prepared by a new phosphate–formate precursor method, *Mater. Chem. Phys.*, 2010, **121**, 370.

41 K. Su, F. Liu and J. T. Chen, Preparation of high performance carbon-coated $LiMnPO_4$ nanocomposite by an acetate-assisted antisolvent precipitation method, *J. Power Sources*, 2013, **232**, 234.

42 H. C. Dinh, S. I. Mho, Y. K. Kang and I. H. Yeo, Large discharge capacities at high current rates for carbon-coated $LiMnPO_4$ nanocrystalline cathodes, *J. Power Sources*, 2013, **244**, 189.

43 Y. B. Cao, J. G. Duan, G. R. Hu, F. Jiang, Z. D. Peng, K. Du and H. W. Guo, Synthesis and electrochemical performance of nanostructured $LiMnPO_4$/C composites as lithium-ion battery cathode by a precipitation technique, *Electrochimica Acta*, 2013, **98**, 183.